THE JOURNAL OF PHYSICAL CHEMISTRY B

Article

pubs.acs.org/JPCB

Car–Parrinello Simulation of the Vibrational Spectrum of a Medium Strong Hydrogen Bond by Two-Dimensional Quantization of the Nuclear Motion: Application to 2-Hydroxy-5-nitrobenzamide

Mateusz Brela,[†,§,+] Jernej Stare,[†,+] Gordana Pirc,[†] Marija Sollner-Dolenc,[∥] Marek Boczar,[§] Marek J. Wójcik,[§,⊥] and Janez Mavri*[,†,‡]

[†]Laboratory for Biocomputing and Bioinformatics, National Institute of Chemistry, Hajdrihova 19, SI-1000 Ljubljana, Slovenia

[‡]EN-FIST Centre of Excellence, Dunajska 156, SI-1000 Ljubljana, Slovenia

[§]Faculty of Chemistry, Jagiellonian University, Ingardena 3, 30-060 Kraków, Poland

[∥]Faculty of Pharmacy, University of Ljubljana, Aškerčeva cesta 7, SI-1000 Ljubljana, Slovenia

ABSTRACT: The nature of medium strong intra- and intermolecular hydrogen bonding in 2-hydroxy-5-nitrobenzamide in the crystal phase was examined by infrared spectroscopy and Car–Parrinello molecular dynamics simulation. The focal point of our study was the part of the infrared spectra associated with the O–H and N–H stretching modes that are very sensitive to the strength of hydrogen bonding. For spectra calculations we used an isolated dimer and the fully periodic crystal environment. We calculated the spectra by using harmonic approximation, the time course of the dipole moment function as obtained from the Car–Parrinello simulation, and the quantization of the nuclear motion of the proton for an instantaneous snapshot of the structures in one and two dimensions. Although quantitative assessment of the agreement between the computed and experimental band contour is difficult due to the fact that the experimental band is very broad, we feel that the most reasonable qualitative agreement with the experiment is obtained from snapshot structures and two-dimensional quantization of the proton motion. We have also critically examined the methods of constructing the one-dimensional proton potential. Perspectives are given for the treatment of nuclear quantum effects in biocatalysis.

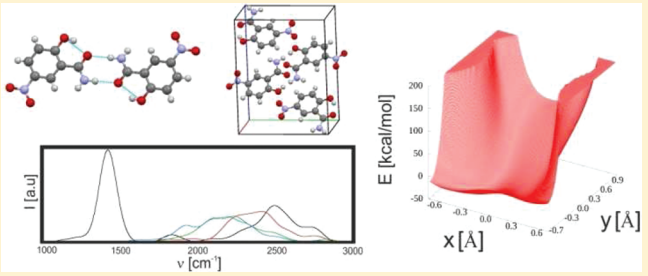

INTRODUCTION

The hydrogen bond (H-bond) is one of the most important interactions in chemical and biochemical systems. The literature concerning progress in hydrogen bonding research is numerous, and it is estimated that over 700 new articles are published each year. The properties of H-bonds have been widely investigated theoretically and experimentally and have been the subject of several monographs and review articles.[1−11] Many theoretical models have been proposed to describe unusual features of hydrogen bonds stretching bands in the IR spectra.[8−10,12−28] As hydrogen bonding is one of the most important interactions in biochemical systems, hydrogen bond dynamics is of great importance for determining H-bond characteristics and functionality.

Any attempt to characterize the properties of chemical or biochemical systems must describe precisely and accurately the interactions in chemical or biochemical systems. The aims of such studies are an explanation of drug action, a detailed description of the biological reactions involved, and an understanding of the nature of proton mobility. 2-Hydroxy-5-nitrobenzamide is one of the derivatives of the biologically active compound benzamide.[29] This compound is currently being studied as an inhibitor of cycloxygenase, an enzyme involved in initiating the inflammation process via the synthesis of prostaglandins. The potential pharmacological use of 2-hydroxy-5-nitrobenzamide justifies our interest in studying the properties of the hydrogen-bonded dimers of 2-hydroxy-5-nitrobenzamide present in the unit cell of the crystal. There are four molecules forming hydrogen-bonded dimers in the crystal structure. Such a system allows us to describe important intra- and intermolecular interactions. Although the conditions in a crystal are not equivalent to those in a living cell—namely our calculations are biased by the artificial periodicity enforced by the calculation which is absent in a biological system—there is at least similarity at the fundamental level, namely that the hydrogen bond dynamics is controlled by a polar and fluctuating environment.

The crystal structure of 2-hydroxy-5-nitrobenzamide was determined using the X-ray diffraction technique of Raza et al.[30] The crystal belongs to the $P2_1/n$ space group. The four molecules create a monoclinic unit cell with parameters a = 5.1803 Å, b = 11.1037 Å, c = 13.7214 Å, and β = 100.642°. In the unit cell, there are four 2-hydroxy-5-nitrobenzamide molecules, each featuring moderately short ($R_{O\cdots O}$ = 2.5196

Received: September 30, 2011
Revised: March 8, 2012
Published: March 19, 2012

   dx.doi.org/10.1021/jp2094559 | J. Phys. Chem. B 2012, 116, 4510–4518

Å) intramolecular hydrogen bonds of the O−H···O type, with each molecule being a donor and acceptor of one relatively long ($R_{N\cdots O}$ = 2.8807 Å) N−H···O bond, forming separated cyclic hydrogen-bonded dimers within the crystal lattice (Figure 1B and C).

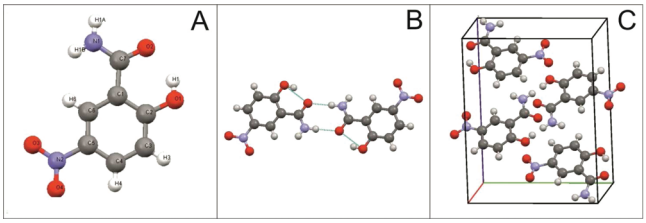

Figure 1. Structure of the 2-hydroxy-5-nitrobenzamide monomer (A), dimer (B), and crystal unit cell (C). Atom colors: grey is carbon, red is oxygen, blue is nitrogen, and white is hydrogen.

Calculations of the vibrational spectra of the H-bonded system are difficult because of large anharmonicity and proton delocalization.[31] Numerical solving of the vibrational Schrödinger equation in at least one dimension is necessary to reproduce the dynamic properties reflected in the vibrational spectra; however, evidence exists that the one-dimensional approach is not sufficient in many cases and that more complex treatment is required.[32−34]

The aim of this work was a calculation of the vibrational spectrum of an H-bonded system of 2-hydroxy-5-nitrobenzamide in the crystalline solid state. In the first step, we optimized the geometry of the unit cell of 2-hydroxy-5-nitrobenzamide, and then we calculated the trajectory using the Car−Parrinello molecular dynamics (CPMD) scheme. CPMD calculations have recently become a popular tool for interpretation of the infrared spectra of hydrogen-bonded systems.[35−41]In the present work we took into account the periodicity of the crystal and thermal fluctuations. The second step involved quantization of the proton motion, for which we used an alternative method based on an *a posteriori* quantization of the nuclear degrees of freedom associated with proton dynamics.

In this paper, we present the results of *ab initio* Car−Parrinello molecular dynamics calculations[42] performed for the unit cell of a 2-hydroxy-5-nitrobenzamide crystal. The vibrational spectrum of the 2-hydroxy-5-nitrobenzamide crystal has been calculated, analyzed, and compared with experimental data and also with the results of DFT calculations performed on an isolated dimer of 2-hydroxy-5-nitrobenzamide. The largest emphasis has been placed on the reconstruction of the stretching bands of hydrogen bonded O−H and N−H groups. The υ_{O-H} and υ_{N-H} bands, obtained from CPMD calculations and instantaneous one- and two-dimensional snapshot potentials, extracted from the trajectory calculated using the Wannier functions,[43] were compared with the experimental bands of the 2-hydroxy-5-nitrobenzamide crystal. We focused only on the ^{1}H isotopomer; isotopically substituted molecules are not considered in the present work.

The methodology for an *a posteriori* quantization of the nuclear motion was developed by the coauthors of this work, and although it provides a rather simplified and inexpensive model of proton dynamics, it yields reasonable agreement between the calculated band contours of the hydrogen bond and the observed features in the spectra; the protocol was successfully applied to hydrogen bonds of different strengths and in various phases. Most of our past experience relied on *one-dimensional* potentials calculated from the snapshot structures (*vide infra*). While Jezierska and Panek[44] eventually utilized a two-dimensional treatment of the hydrogen bond dynamics, it was solely used for the calculation of the potential of mean force. Recently Kühn and co-workers applied a similar strategy based on one- and two-dimensional snapshot potentials of a molecular dynamics (MD) trajectory in their studies of pump−probe spectra of nucleic acid base pairs in solution.[45,46] Additionally, Corcelli and Skinner calculated infrared and Raman line shapes of HOD in liquid H_2O and D_2O by using snapshot structures and the correlation between the instantaneous electric field of the solvent and the pertinent vibrational frequency and intensity.[47]

The snapshot methodology utilized in this study represents an effort to improve classical molecular dynamics simulation, by quantizing selected nuclear degrees of freedom, and to elaborate the influence of the quantum nature of nuclear motion on the resultant spectroscopic properties. In this sense, the present methodology can be compared to the established protocols of mixed quantum-classical dynamics, which provide time-resolved quantization of the selected nuclear degrees of freedom. Examples of mixed quantum-classical dynamics methodologies are the "molecular dynamics with quantum transitions" (MDTQ)[48,49] and "quantum wavepacket ab initio molecular dynamics" (QWAIMD)[32] approaches, developed by Hammes-Schiffer and Iyengar, respectively. Clearly, these methodologies represent a superior approach of computing a three-dimensional nuclear time-dependent wave function and other quantum properties at every instant during the course of a MD simulation. Importantly, mixed quantum-classical dynamics techniques feature on-the-fly computed interaction between the quantum wavepacket and its classical surroundings, which is implemented in the MD protocol. In this sense, our snapshot methodology is by far more approximative, because it neglects these effects or it considers the quantum-dynamical aspect. In our approach instantaneous proton potentials are computed on a pre-existing MD trajectory, and nuclear quantum effects are assessed only by a time-independent formalism. While our approach is evidently less accurate, it features a benefit of relatively low computational cost and, importantly, can be easily used with virtually any existing ab initio MD code (CPMD in the present case) with no modification. Quantization of nuclear motion is a valuable tool for studies of factors responsible for enzyme catalysis.[50] Recent advances in the QWAIMD methodology, such as application to enzyme active sites,[33] support for the QM/MM protocol,[49] and support for periodic boundary conditions with exploited symmetry features,[34] indicate that the methodology is evolving into a powerful tool for time-resolved treatment of nuclear quantum effects even in very complex systems in the condensed phase.

The organization of this article is as follows. Section 2 presents computational methods, section 3 contains results and discussion, and concluding remarks are outlined in section 4.

■ COMPUTATIONAL METHODS

Geometry optimizations and vibrational frequency calculations were performed to characterize the key stationary points on the potential energy surface (PES) for the 2-hydroxy-5-nitrobenzamide dimer (Figure 1B) using the Gaussian 03 program package.[50] In all static dimer calculations, Pople's basis sets have been used with polarization and augmented with diffuse

dx.doi.org/10.1021/jp2094559 | J. Phys. Chem. B 2012, 116, 4510−4518

functions (6-311++G(d,p)) for two functionals: B3LYP and B3PW91. We have also performed a vibrational analysis in the optimized crystal structure[30] using the CPMD program package version 3.13.2.[51] The BLYP[52] density functional together with a plane-wave basis set with a kinetic energy cutoff of 200 Ry was used in our study. The Goedecker atomic pseudopotentials[53] were used for the treatment of the core electrons. The Γ-point approximation was adopted in the calculation of the integrals in the reciprocal space, among the rest because the Car−Parrinello molecular dynamics approach (see below) is limited to the Γ-point approximation. Test calculations of energy and forces gave evidence that the error due to the incomplete *k*-point sampling is at most of the same magnitude as the uncertainty due to the choice of pseudopotentials or to the incomplete plane-wave basis set.

The starting point for our molecular dynamics (MD) simulation was the X-ray structure data obtained by Raza et al.[30] The unit cell contains four equivalent H-bonded moieties (Figure 1). Three-dimensional periodicity was fully implemented in our calculation. The MD simulation was carried out in the unit cell fixed to the experimentally determined size and shape and using the Car−Parrinello scheme.[42] The fictitious orbital mass was set to 400 au, and the molecular dynamics time step was set to 2 au (about 0.048 376 fs), while other properties were set the same as those for the static calculation. The temperature was set to 300 K by means of a Nosé−Hoover thermostat with a coupling frequency of 1500 cm^{-1}. The total simulation time was about 5 ps. The simulation was performed on an HP Cluster Platform 3000 BL 2 × 220 PC/LINUX, and it lasted for about 180 days using 12 CPU cores.

The anharmonic vibrational spectrum was calculated using the Fourier transformation of the dipole autocorrelation function obtained from dipole trajectories generated by the CPMD simulation facilitated by the scripts of Kohlmeyer.[54] The dipole trajectory was calculated using the optimally localized Wannier functions.[55]

Snapshot structures of the trajectory were extracted every 4000 steps (about 194 fs), yielding 30 distinct structures, representative of the fluctuating crystalline environment. Note that due to the fact that four molecules exist in the unit cell, the total number of distinct hydrogen bonded moieties extracted was 120. The contour of the O−H stretching band was then calculated using three distinct strategies, differing only in the calculation of the proton potentials. For each of the extracted snapshot structures, one-dimensional (1D) proton potential functions were obtained by stepwise displacement of one hydrogen-bonded proton along the selected coordinate. Three distinct coordinates were chosen in our study. In the first case (I), the hydrogen was displaced along the vector parallel to the pertinent O···O line in 0.1 Å steps. The corresponding internal coordinate (x) was defined as the longitudinal projection of the proton position to the line passing through both oxygen atoms, and the origin was set to the midpoint between the oxygens (Figure 3). The scan typically covered the x range between −0.3 and 0.7 Å. In the second case (II), hydrogen was displaced along the vector parallel to the pertinent O−H line (Figure 2) in 0.1 Å steps. The corresponding internal coordinate (x) was defined as the distance between hydrogen and oxygen atoms. The scan typically covered the x range between −0.2 and 0.8 Å. In the third case (III), the hydrogen was displaced along the arc defined by the O−H···O circle (Figure 2) in angular steps of 4% of the arc length. The corresponding internal coordinate (x) was a fraction of the arc at which the proton was located,

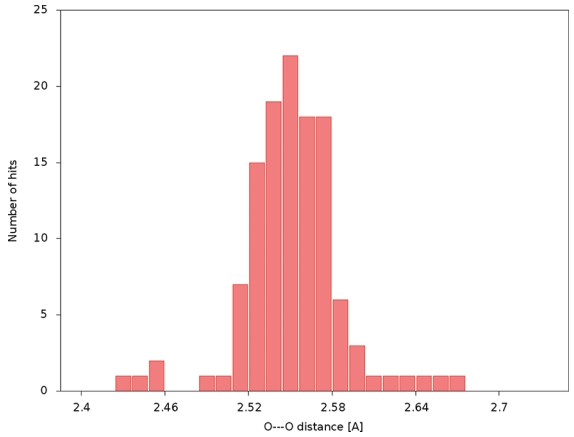

Figure 2. Distribution of the O···O distance in a strong hydrogen bond extracted from snapshot structures of the CPMD simulation represented by histograms. The applied bin width was 0.01 Å.

where the donor oxygen was, by definition, set to be at $x = 0$ and the acceptor oxygen at $x = 1$. The range of x in a typical scan was between 0.20 and 0.76. In the way described above, three sets of 120 distinct proton potentials were calculated, each set corresponding to a different internal coordinate in which the vibrational problem was formulated and solved.

In addition to the 1D scans, we also calculated 120 2D proton potential functions for the corresponding 120 O−H···O snapshot moieties. The potentials covered both the longitudinal ("stretching") and transversal ("bending") motions of the proton. They were obtained by stepwise displacement of one of the H-bonded hydrogens in two directions: the first coordinate representing the longitudinal proton motion parallel to O···O (x) was defined in the same way as that in the 1D potential (I) presented above, while the transversal coordinate (y) was perpendicular to x. Such a choice of internal coordinates is suitable for large-amplitude proton motion and also for the cases when the proton exhibits the affinity to be located near the acceptor site of the H-bond. Additionally, this coordinate set benefits from a very simple form of kinetic energy terms in the vibrational Hamiltonian. A similar choice of a 2D coordinate system has been used in the past for the quantum treatment of a H-bonded proton, yielding good results.[56]

The N−H stretching band of both N−H groups in the molecule (of which one is involved in an intermolecular N−H···O group while the other one is free) was elaborated in a similar manner by calculating the 1D stretching potentials for the snapshot structures. Here, only the N−H distance was used as the control variable, and the proton was displaced along the N−H bond line in the same manner as described for potential II for the O−H···O moiety.

All proton potential calculations presented above were of a single point type; that is, during the scan all other atoms were fixed. This approximation implies that the motion of the O−H and N−H groups is much faster than vibrations along the other degrees of freedom. The typical 2D proton potentials for O−H modes obtained from snapshot structures are shown in Figure 3.

Having acquired the potentials, the vibrational energy levels and proton wave functions were obtained by solving the vibrational Schrödinger equation for each individual potential. The variational Fourier grid Hamiltonian method adapted for application in generalized internal coordinates was used for this

dx.doi.org/10.1021/jp2094559 | J. Phys. Chem. B 2012, 116, 4510−4518

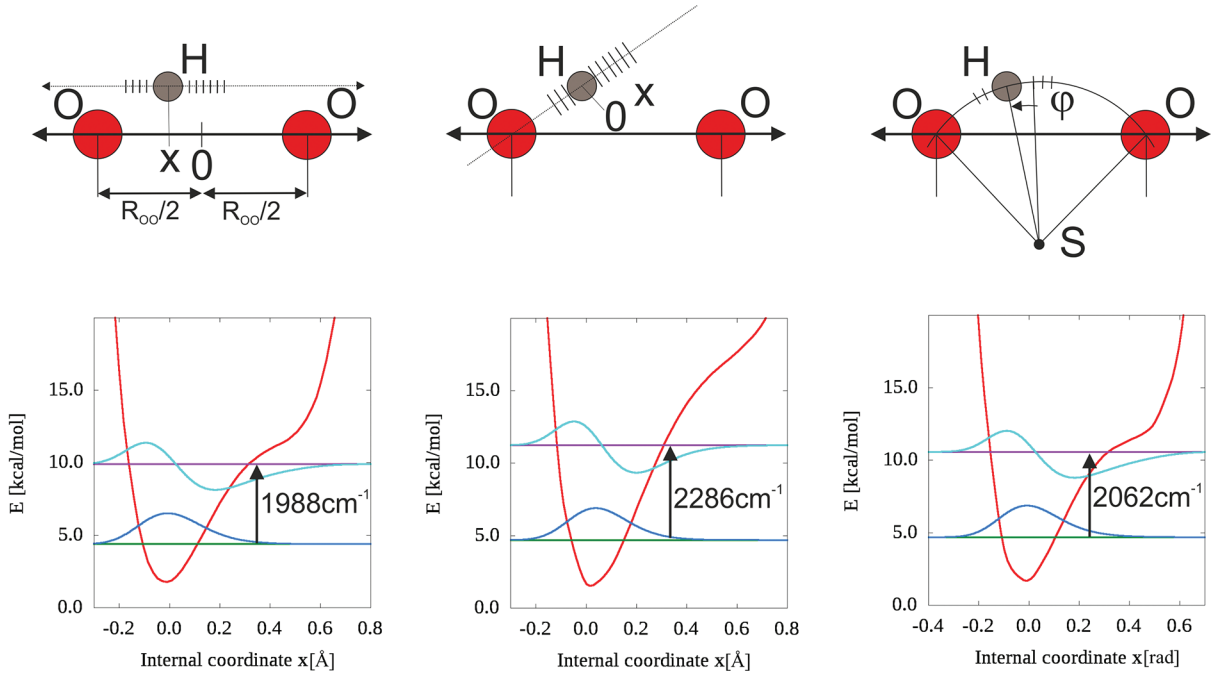

Figure 3. Definition of pathways for one-dimensional proton potentials (upper figures). The lower figures show the corresponding proton potentials with the first two eigenvalues and eigenfunctions. All three proton potentials were obtained from the same snapshot structure.

purpose. Sample 2D wave functions corresponding to the ground state and first excited state are shown in Figure 3.

As each instantaneous snapshot structure yields its own potential and a characteristic anharmonic frequency, the superposition of the calculated frequencies represents the contour of the corresponding band in the spectrum. When calculating the contours of the N−H/O−H bands from 1D potentials, we considered only the fundamental (0 → 1) transition for each proton potential. The contour of the band was obtained as a set of lines, each line corresponding to one 0 → 1 transition calculated from its snapshots potential. To simulate a continuous spectrum, we overlapped each transition by a Gaussian with an arbitrary half-width of 50 cm^{-1}, and the continuous function was obtained by summing the Gaussians. For the contour calculated from the 2D snapshot potentials, both 0 → 1 and 0 → 2 transitions were considered; the former corresponds to the in-plane O−H bending excitations, while the latter represents the O−H stretching. The contribution of bending overtones (most of which are located in the 2800−3000 cm^{-1} region) to the visualized spectrum was neglected due to presumed low intensity; however, potential interactions between bending overtones and stretching fundamentals (which are not expected to be significant due to a frequency separation of several hundred wavenumbers) have been included in the protocol for solving the 2D Schrödinger equation. Spectra obtained by this procedure are shown in Figures 4 and 5 for 1D and for 2D proton potentials, respectively.

It should be noted that in this study we focused only on isotopically unsubstituted molecules.

Experimental Section. Fourier-transform infrared (FTIR) spectra of the prepared glasses were obtained with an FTIR spectrometer (Perkin-Elmer 1600 FT-IR spectrometer). Powdered samples were mixed with KBr powders and pressed to form thin transparent disks whose IR spectra could be observed. Infrared absorption spectra within the range 450−4000 cm^{-1} were recorded at room temperature.

RESULTS AND DISCUSSION

A. Geometry Analysis. The results of our study are presented in the following order: analysis of the structure, construction of the potential energy surface, and vibrational analysis. Figure 1 shows the structure of the 2-hydroxy-5-nitrobenzamide monomer. The monomers form cyclic symmetric dimers (Figure 1) stabilized by four hydrogen bonds, of which two intramolecular hydrogen bonds are stronger and two intermolecular hydrogen bonds are weaker. The calculated 2-hydroxy-5-nitrobenzamide dimer geometry parameters are in good agreement with the experimental data.

Analysis of the Car−Parrinello trajectory shows a time-course of the O···O and O−H distances in the O−H···O moiety and shows that the proton is asymmetrically located nearer to the donor oxygen. The time-averaged O···O distance is 2.56 Å, ranking the H-bond among medium strong ones; the value is slightly longer than the experimental crystallographic distance of 2.52 Å. The distribution of the O···O distance, sampled by the extracted snapshot structures, resembles Gaussian shape and is in fair agreement with the time-averaged value (Figure 2).

The diffraction experiment[30] gave an O−H distance of 0.82 Å, which is notably underestimated for known reasons associated with the limitations of X-ray diffraction.[57] Our CPMD simulation predicts that this bond is longer, with an average bond length of 1.035 Å. The X-ray diffraction measurement thus underestimates the O−H distance in the hydrogen-bonded 2-hydroxy-5-nitrobenzamide. Our CPMD simulation reproduces the geometric parameters for hydrogen bonds in the crystal reasonably well.

B. Infrared Spectra of Dimer and Crystal Structures Calculated in the Harmonic Approximation. The experimental infrared spectrum of the 2-hydroxy-5-nitro-

dx.doi.org/10.1021/jp2094559 | J. Phys. Chem. B 2012, 116, 4510−4518

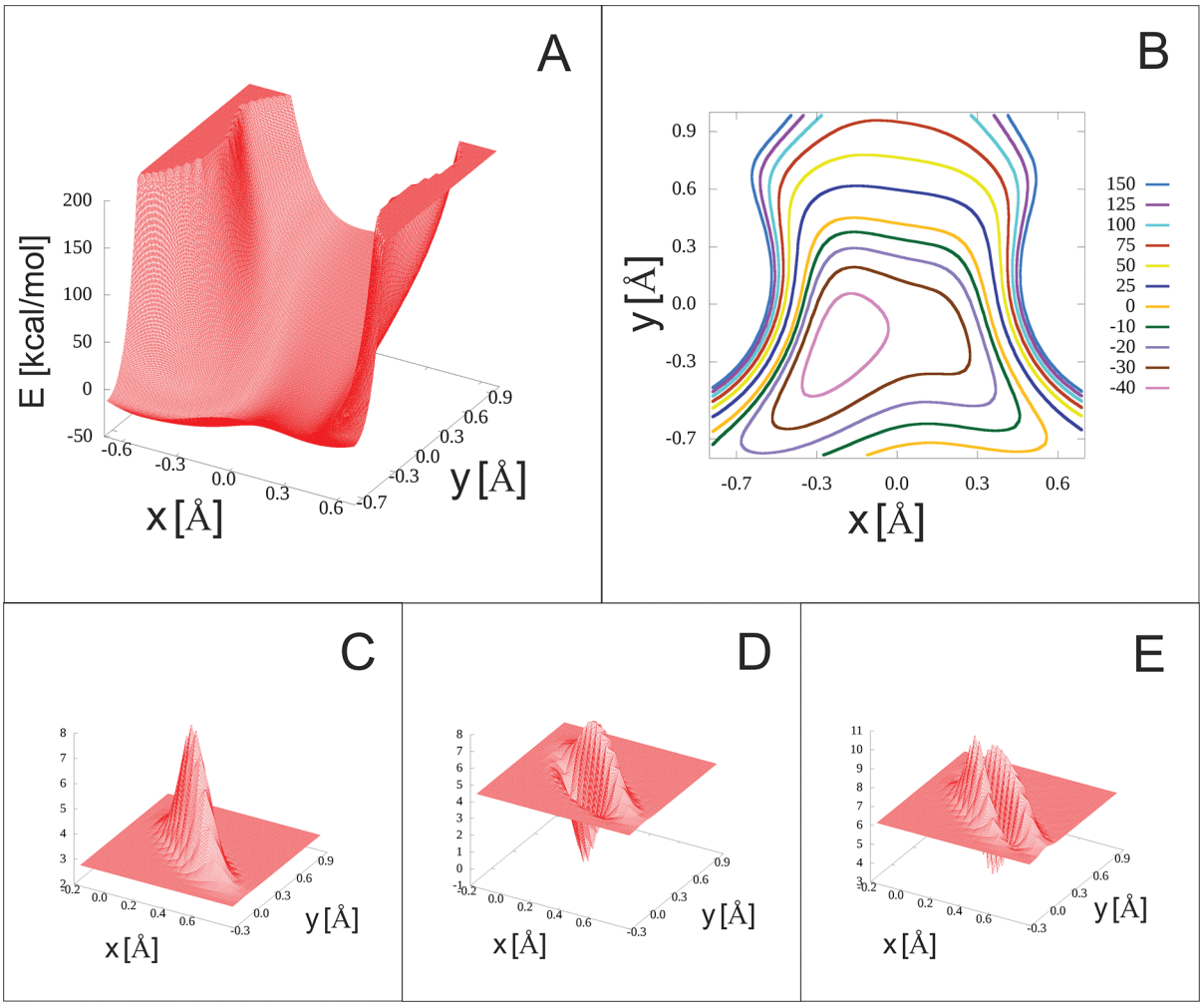

Figure 4. Sample 2D proton potential: surface plot (A) and contour map (B; the energy values (relative to the minimum) pertaining to the contours are given in kcal/mol). *x* is the coordinate of the proton motion along the O···O vector, while *y* is the coordinate of the proton motion perpendicular to the O···O vector. Wave functions of the first three vibrational states are shown in parts C, D, and E.

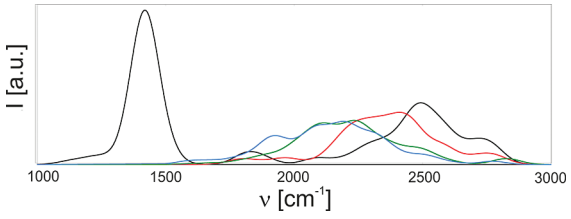

Figure 5. O−H stretching envelopes calculated from the individual fundamental vibrational transitions as a superposition of Gaussian functions with a half width of 50 cm^{-1}. The proton potential was constructed by displacing the proton either (I) along the line parallel to the O···O vector (green line), (II) along the OH vector (red line), or (III) along the circular pathway (blue line). The black line represents the combined O−H stretching/bending envelope derived from 2D snapshot potentials. For a detailed description of the modeling of proton motion, see Figure 2 and the text.

benzamide crystal is shown in Figure 6A and compared with the DFT calculated dimers spectra (Figure 6B) and crystal spectrum (Figure 6C), both calculated in the harmonic approximation. The dimer spectra are composed of three peaks, centered at 3202 (3260 cm^{-1} for B3LYP calculation), 3367, and 3712 cm^{-1}. They represent O−H stretching, hydrogen-bonded N−H stretching, and free N−H stretching, respectively. They reproduce qualitatively the experimental bands, though their positions are shifted to lower frequencies for the N−H bands and to a higher frequency for the O−H band. The harmonic crystal spectrum exhibits three major peaks centered at 2689, 3253, and 3400 cm^{-1}. The agreement with the experimental broad massif of the spectrum with a maximum at 2500 cm^{-1}, which represents the O−H stretching band, is better in this case than in the dimer calculation. Harmonic calculations reproduce the positions and intensities of the O−H and N−H stretching vibrations reasonably well; however, the calculated spectra do not reproduce the broadening and intensity increase caused by the anharmonic inter- and intramolecular couplings present in hydrogen bonds.[2] In harmonic quantum chemical calculations one does not obtain bandwidths, and vibrational transitions are represented by δ functions. The band shapes presented in Figure 6B and C were obtained by superimposing a Gaussian function with a half-width 50 cm^{-1} on each calculated transition; such representations have often been used, for example in refs 14 and 58−61.

C. Infrared Spectrum from the Dipole Moment Autocorrelation Function. The infrared spectrum calculated by Fourier transformation of the dipole autocorrelation function calculated from the dipole moment trajectory of the

dx.doi.org/10.1021/jp2094559 | J. Phys. Chem. B 2012, 116, 4510−4518

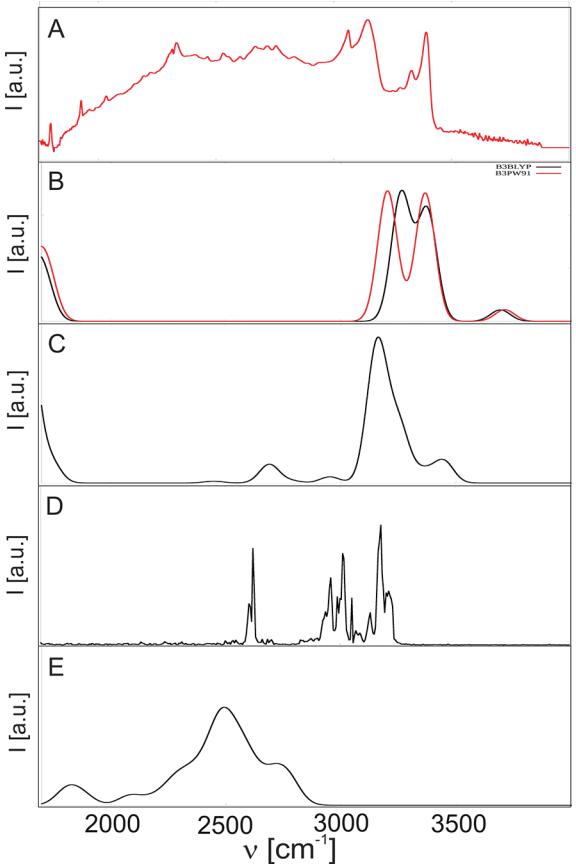

Figure 6. Infrared spectra (or selected band contours) of 2-hydroxy-5-nitrobenzamide. A is the experimental spectrum, B the dimer spectrum calculated in the harmonic approximation, C the crystal calculated in the harmonic approximation, D the spectrum calculated by the Fourier transform of the dipole moment from the Car–Parrinello trajectory, and E the O–H stretching/bending contour obtained from the 2D snapshots proton potential.

CPMD simulation is shown in Figure 6D. The pattern of bands is qualitatively quite similar to the one obtained from harmonic CPMD frequency calculation on the periodic model (Figure 6C), but it is slightly shifted to lower frequencies. Given that the MD simulation is performed in the on-the-fly computed periodic DFT force field, which includes anharmonic effects, the downshift of frequencies is not surprising, because anharmonicity typically flattens the potential energy surface and lowers the frequency. Yet, this effect does not appear to be significant, particularly because the experimental band spans a much wider range, and not much can be concluded about the agreement between the calculated and observed spectral patterns. Although the calculated spectrum fits qualitatively into the band, it considerably underestimates its breadth. The latter can be at least in part attributed to the fact that no nuclear quantum effects were undertaken in the calculation of the spectrum. Some recent studies of vibrational band shapes of H-bonded systems (water clusters, hydrated hydroxide anion, hydrated hydroperoxyl radical, protonated dimethyl ether dimer in the gas phase) have been performed by advanced Fourier transform techniques,[35,62,63] and some of them feature superior agreement with available experimental data.[61] It should also be noted that the discrepancy between the calculated and observed band contours may not only be due to nuclear quantum effects but also to a number of approximations or uncertainties inherent to the methodology employed in this study, among the rest the Γ-point approximation, incomplete basis set, pseudopotential approximation, etc.

D. Snapshot Potential Energy Functions. We calculated 1D and 2D proton potentials corresponding to the instantaneous snapshot structures extracted from the CPMD trajectory. Construction of the 1D proton potentials for several snapshots is computationally much more affordable than the 2D treatment. It should be noted that while a typical 1D scan requires 10–15 points at which the energy is evaluated, a 2D scan requires about 200–400 points; the number of potential energy evaluations increases exponentially with the dimensionality of the vibrational problem. Construction of the 2D surfaces for several snapshots is computationally demanding and as such it is not practical for routine computational interpretation of spectroscopic data. Nevertheless, in the context of the QWAIMD mixed quantum-classical dynamics protocol, notable improvement in efficiency of the potential energy surface sampling is achievable through the time-dependent deterministic sampling (TDDS) routine,[32] particularly for a full three-dimensional treatment of the wavepacket, making it a challenging tool for future studies.

We compared the bands calculated with the three different choices of the internal coordinate, and the choice of coordinate for the modeling of proton motion proved to be a critical element of the simulation.

We generated one-dimensional proton potentials using two linear pathways and one circular pathway. Figure 3 shows schematically the construction of the proton potential and the corresponding potentials together with the two lowest vibrational energy levels and proton wave functions. All three potentials were obtained from the same snapshot structure. The fundamental transition has the highest frequency for the proton potential obtained by simple elongation of the O–H bond (2286 cm^{-1}) (potential II) and the lowest for the parallel motion along the parallel to the O···O vector (1988 cm^{-1}) (potential I). The circular motion (potential III) yields the fundamental of 2062 cm^{-1}, quite close to the value obtained for the parallel motion. The corresponding 2D proton potential is shown in Figure 4. Its shape and analysis of the wave functions give evidence for coupling between stretching and bending modes. The frequency of the O–H stretching has a value of 2443 cm^{-1}. This value is in good agreement with the frequency obtained by the proton potential constructed by elongation of the O–H bond length. The same is true for a large majority of the potentials calculated from the other snapshots. These results indicate that the best 1D potential to reproduce experimental spectra is obtained by elongation of the proton along the O–H vector. Perhaps this is not a surprise, since in the moderately strong and weak hydrogen bonds the proton stretching motion is most often a simple linear elongation and shortening of the bond between hydrogen and the donor atom; coupling to other modes and deviations from linearity are much less common than in short, strong hydrogen bonds.[64] Construction of the two-dimensional surfaces for several snapshots is computationally demanding, and as such, it is not practical for routine computational interpretation of spectroscopic data.

E. Analysis of the Snapshot Band Contours. We calculated part of the spectrum associated with the O–H motion. The spectrum was obtained by solving the vibrational Schrödinger equation using all above-described potentials for the snapshots. The spectrum is shown in Figure 5. More than

dx.doi.org/10.1021/jp2094559 | J. Phys. Chem. B 2012, 116, 4510–4518

90% of frequencies, which were calculated by using the three types of 1D potentials, span the range from 1400 to 2800 cm^{-1}. The contour of the band depends on the choice of the proton movement pathway. In general, snapshot proton potentials constructed following the O−H direction are shifted to higher frequencies than those of the longitudinal and circular proton pathway model (potentials I and III). This strategy also yields a narrower band contour with a half-width of about 387 cm^{-1}. When we use the model of the proton pathway parallel to the O···O direction and the circular pathway, the band contours are very similar to each other. The main difference is a red shift of about 200 cm^{-1} relative to the band calculated by plain elongation of the O−H bond and preserving the bond angle. The narrower O−H band obtained by the latter strategy can be explained by the lower sensitivity of the proton potential to the fluctuations of the environment, resulting in the fact that the potentials—and thus the frequencies—are less diverse than in the other two cases. The estimated half-widths of the spectra shown in Figure 5 are 387 cm^{-1} for elongation of the O−H bond, 400 cm^{-1} for the pathway parallel to the O···O vector, and 600 cm^{-1} for the circular pathway. Circularly constructed proton potentials probably exhibit traces of the bending motion in the corresponding band, because a circular proton motion includes by definition a small contribution by the O−H bending mode. Nevertheless, the feature of the contour that could be attributed to the bending component appears at about 1900 cm^{-1}, which is beyond a reasonable range for a regular bending mode; eventually it is located about 400 cm^{-1} higher than the centroid of the O−H bending mode obtained by the 2D treatment.

The band contours calculated from 1D potentials are compared with those obtained from 2D potentials in Figure 5. In the part related to OH stretching, the center of the 2D calculated contour is shifted to higher frequencies by about 100−300 cm^{-1} (depending on the 1D model pathway to which it is compared); the band calculated from 1D potentials obtained by plain O−H bond elongation gives the best agreement with the 2D treatment. Qualitatively, the 2D contour is closer to the center of the experimental broad absorption (the 1D contours are near the low frequency limit), but given that the experimental band eventually covers a much wider range (also incorporating CH and NH stretching bands not undertaken in the present study), it cannot be safely deduced that the 2D treatment yields significantly better agreement with the experimental spectrum.

At this point it should also be noted that the significant dependence of the computed band contour on the choice of the coordinate in which the vibrational problem is formulated indicates that the 1D modeling of proton motion is to a certain extent insufficient. Additionally, validation of the employed computational strategy by comparison with the experimental spectrum is rather difficult because the corresponding experimental band is extremely broad and partially overlapped with bands not considered by our calculations. Thus, it remains a challenge to employ a superior multidimensional methodology such as mixed quantum-classical dynamics.[34] An advantage of the mixed quantum-classical methodology is also the fact that it accounts for the time-resolved coupling between the quantized hydrogen and its environment.

To provide a more complete picture of the hydrogen bond spectra in 2-hydroxy-5-nitrobenzamide, we also considered the N−H motion. One N−H proton is involved in the N−H···O hydrogen bonding, while the other one is free. We applied the snapshots methodology, as it was used for the O−H treatment, and the proton potentials were constructed by linearly displacing the N−H bond lengths with a fixed bond angle. The calculated band contours are shown in Figure 7. To calculate both bands, we used the one-dimensional Schrödinger equation. The center of the N−H stretching band involved in hydrogen bonding is 2917 cm^{-1}, and its half-width is 160 cm^{-1}. The corresponding values for free N−H stretching are 3158 and 146 cm^{-1}. They are in reasonably good agreement with the experimental values. The experimentally assigned center of the hydrogen-bonded N−H stretching vibration is at 3130 cm^{-1}, and its half-width is 200 cm^{-1}, while for the N−H of the free group the center is at 3400 cm^{-1} and the half-width is 100 cm^{-1}. The red-shifted band has an asymmetric shape that represents the typical situation for hydrogen-bonded systems. In contrast to that, the nonbonded N−H group has a much more symmetric band.

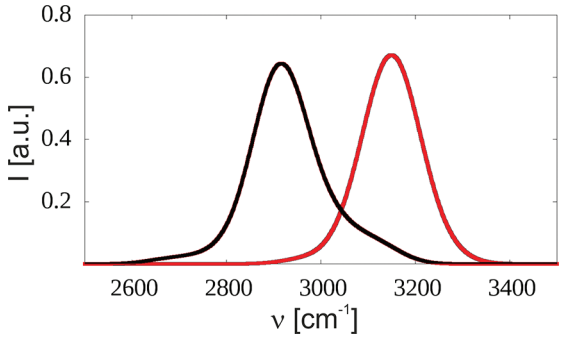

Figure 7. N−H stretching envelopes calculated from the individual fundamental vibrational transitions as a superposition of Gaussian functions with a half width of 50 cm^{-1}. The black line represents the band corresponding to the N−H group involved in hydrogen bonding, while the red line represents the free N−H group. For a detailed description of the calculation, see Figure 2 and the text.

CONCLUSIONS

In this article we examined the nature of medium−strong intermolecular hydrogen bonding in 2-hydroxy-5-nitrobenzamide in the crystal phase. In particular, we were interested in the parts of the infrared spectra associated with O−H and N−H stretching modes that are very sensitive to the strength of hydrogen bonding. Our experimental work was supported by a variety of calculations, based on DFT modeling, which included harmonic analysis, Car−Parrinello molecular dynamics simulation, and quantization of the proton motion in the instantaneous potentials influenced by the fluctuating environment. Frequencies calculated for an isolated dimer in the harmonic approximation show poor agreement with the experiment. Inclusion of the crystal field in conjunction with the harmonic approximation improves the results. Additional improvement was obtained by Fourier transform of the time course of the dipole moment function from the Car−Parrinello trajectory. This approach included thermal fluctuations but no quantization of the O−H or N−H motion. Reasonable agreement with the experiment was obtained by solving the Schrödinger equation for the snapshots of the 1D and 2D proton potentials. We also considered the influence of the chosen internal coordinate for the representation of the 1D vibrational problem and found that the potential constructed by the plain elongation of the O−H bond length gives the best

dx.doi.org/10.1021/jp2094559 | J. Phys. Chem. B 2012, 116, 4510−4518

agreement with the 2D treatment and, qualitatively, reasonable agreement with the experimental spectrum.

Comparison of the computed band frequencies and contours with the experimental data reveals the limitation of the applied computational techniques. Namely, due to the fact that the observed band attributed to the O−H stretching mode is notably broader than any calculated contour, it is very difficult to validate the employed computational strategies. Most of the computed band contours fit qualitatively into the observed absorption—the 2D envelope appears to fit slightly better than bands calculated from 1D snapshot potentials, but neither model is capable of reproducing the experimental bandwidth of over 1000 cm^{-1}. Nevertheless, it is clear that inclusion of nuclear quantum effects contributes to significant broadening of the OH stretching band, thus providing better agreement with the experiment than Fourier transformation of the dipole moment autocorrelation function. A challenge remains for an improved treatment by advanced methodologies such as mixed quantum-classical dynamics techniques.[34]

The treatment of nuclear quantum effects presented in this work has possible application in biocatalysis. Providing valuable information on catalytic pathways, nuclear quantum effects represent an important field in enzymology. They include altered geometry parameters, binding affinities, and kinetic isotope (KIE) effects. The most pronounced changes are for H/D substitution; in many cases, large values of KIE indicate the role of tunneling in the catalyzed reaction.[65,66] Our recent experience includes modeling of tunneling by a variety of methods, some of which are closely related to the techniques employed in this work.[67] Thus, further computational research on biomolecular reactions will also benefit from the experience gained in the present study.

AUTHOR INFORMATION

Corresponding Author

*E-mail: janez.mavri@ki.si.

Present Address

⊥Visiting professor at Kyushu University, Japan.

Author Contributions

+Both authors contributed equally to this work.

Notes

The authors declare no competing financial interest.

ACKNOWLEDGMENTS

We are grateful for the use of the "Zeus" supercomputer at Cracow for allocated CPU time. This research was supported in part by PL-Grid Infrastructure (ACC Cyfronet AGH). The authors would also like to thank the Slovenian Research Agency for financial support. This work was carried out within the framework of the program groups with program codes P1-0012 and P1-0010 and within the corresponding research project contracts Nos. J1-2014 and J1-2252. We would like to thank Ms. Charlotte C. W. Taft for linguistic corrections.

REFERENCES

(1) Hadži, D.; Thompson, H. W. International Union of Pure and Applied Chemistry. Hydrogen bonding: papers presented at the Symposium on Hydrogen Bonding held at Ljubljana, 29 July−3 August 1957; Pergamon Press: London, 1959.

(2) Pimentel, G. C.; McClellan, A. L. *The hydrogen bond*; W.H. Freeman; trade distributor: Reinhold Pub. Corp.: New York, San Francisco, 1960.

(3) Schuster, P.; Zundel, G.; Sandorfy, C. *The Hydrogen bond: recent developments in theory and experiments*; North-Holland Pub. Co., American Elsevier Pub. Co.: Amsterdam, NY, 1976.

(4) Scheiner, S. *Hydrogen bonding: a theoretical perspective*; Oxford University Press: New York, Oxford, 1997.

(5) Jeffrey, G. A. *An introduction to hydrogen bonding*; Oxford University Press: New York, Oxford, 1997.

(6) Hadži, D. *Theoretical treatments of hydrogen bonding*; Wiley: Chichester, 1997.

(7) Grabowski, S. J. *Hydrogen Bonding; New Insights*; Springer: Dordrecht, 2006.

(8) Maréchal, Y. In *Molecular Interactions*; Ratajczak, H., Ed.; Wiley: Chichester, 1980; Vol. *1*.

(9) Sandorfy, C. *Top. Curr. Chem.* **1984**, *120*, 41−84.

(10) Henri-Rousseau, O.; Blaise, P. *Adv. Chem. Phys.* **1998**, *103*, 1−186.

(11) Kurczab, R.; Mitoraj, M. P.; Michalak, A.; Ziegler, T. *J. Phys. Chem. A* **2010**, *114* (33), 8581−8590.

(12) Bratož, S.; Hadži, D. *J. Chem. Phys.* **1957**, *27* (5), 991−997.

(13) Maréchal, Y. W. A. *J. Chem. Phys.* **1968**, *48* (8), 3697−3705.

(14) Witkowski, A.; Wojcik, M. *Chem. Phys.* **1973**, *1* (1), 9−16.

(15) Wojcik, M. J. *Int. J. Quantum Chem.* **1976**, *10* (5), 747−760.

(16) Wojcik, M. J. *J. Mol. Struct.* **1978**, *47* (May), 303−306.

(17) Flakus, H. T. *THEOCHEM* **1993**, *104* (3), 281−292.

(18) Ratajczak, H.; Yaremko, A. M. *Chem. Phys. Lett.* **1999**, *314* (1−2), 122−131.

(19) Henri-Rousseau, O.; Chamma, D. *Chem. Phys.* **1998**, *229* (1), 37−50.

(20) Yaremko, A. M.; Ratajczak, H.; Baran, J.; Barnes, A. J.; Mozdor, E.; Silvi, B. *Chem. Phys.* **2004**, *306* (1−3), 57−70.

(21) Blaise, P.; Wojcik, M. J.; Henri-Rousseau, O. *J. Chem. Phys.* **2005**, *122* (6), 064306−1−12.

(22) Sandorfy, C. *J. Mol. Struct.* **2006**, *790* (1−3), 50−54.

(23) Boczar, M.; Boda, L.; Wojcik, M. J. *J. Chem. Phys.* **2006**, *124* (8), 084306−1−12.

(24) Wojcik, M. J.; Boczar, M.; Boda, L. *J. Chem. Phys.* **2006**, *125* (8), 084709−1−13.

(25) Wojcik, M. J.; Boczar, M.; Boda, L. *J. Chem. Phys.* **2007**, *127*, 8.

(26) Wojcik, M. J.; Boczar, M.; Kwiendacz, J. *J. Chem. Phys.* **2008**, *128* (16), 164506−1−12.

(27) Wojcik, M. J.; Boczar, M.; Kurczab, R. *Vib. Spectrosc.* **2010**, *52* (1), 39−47.

(28) Wojcik, M. J.; Kwiendacz, J.; Boczar, M.; Boda, L.; Ozaki, Y. *Chem. Phys.* **2010**, *372* (1−3), 72−81.

(29) Velcheva, E. A.; Stamboliyska, B. A. *J. Mol. Struct.* **2008**, *875* (1−3), 264−271.

(30) Tahir, M. N.; Raza, A. R.; Nisar, B.; Danish, M.; Iqbal, M. S. *Acta. Crystallogr., E* **2009**, *65*, O3260−U2044.

(31) Balintkurti, G. G.; Dixon, R. N.; Marston, C. C. *Int. Rev. Phys. Chem.* **1992**, *11* (2), 317−344.

(32) Sumner, I.; Iyengar, S. S. *J. Phys. Chem. A* **2007**, *111* (41), 10313−10324.

(33) Iyengar, S. S.; Sumner, I.; Jakowski, J. *J. Phys. Chem. B* **2008**, *112* (25), 7601−7613.

(34) Li, X.; Iyengar, S. S. *J. Phys. Chem. A* **2011**, *115* (23), 6269−6284.

(35) Iyengar, S. S.; Petersen, M. K.; Day, T. J. F.; Burnham, C. J.; Teige, V. E.; Voth, G. A. *J. Chem. Phys.* **2005**, *123* (8), 084309-1-9.

(36) Mavri, J.; Jezierska, A.; Panek, J. J.; Koll, A. *J. Chem. Phys.* **2007**, *126* (20), 205101-1-9.

(37) Stare, J.; Panek, J.; Eckert, J.; Grdadolnik, J.; Mavri, J.; Hadzi, D. *J. Phys. Chem. A* **2008**, *112* (7), 1576−1586.

(38) Durlak, P.; Latajka, Z.; Berski, S. *J. Chem. Phys.* **2009**, *131* (2), 024308-1-8.

(39) Durlak, P.; Latajka, Z. *Chem. Phys. Lett.* **2009**, *477* (4−6), 249−254.

(40) Mavri, J.; Pirc, G.; Stare, J. *J. Chem. Phys.* **2010**, *132* (22), 224506-1-7.

(41) Wojcik, M. J.; Kwiendacz, J.; Boczar, M. *Chem. Phys. Lett.* **2011**, *501* (4−6), 623−627.
(42) Car, R.; Parrinello, M. *Phys. Rev. Lett.* **1985**, *55* (22), 2471−2474.
(43) Wannier, G. H. *Phys. Rev. A* **1937**, *52* (3), 7.
(44) Jezierska, A.; Panek, J. J. *J. Chem. Theory Comput.* **2008**, *4* (3), 375−384.
(45) Yan, Y. A.; Kuhn, O. *Phys. Chem. Chem. Phys.* **2010**, *12* (48), 15695−703.
(46) Yan, Y. A.; Kuhn, O. *J. Phys. Chem. B* **2011**, *115* (18), 5254−5259.
(47) Corcelli, S. A.; Skinner, J. L. *J. Phys. Chem. A* **2005**, *109* (28), 6154−6165.
(48) Drukker, K.; Hammes-Schiffer, S. *J. Chem. Phys.* **1997**, *107* (2), 363−374.
(49) Sumner, I.; Iyengar, S. S. *J. Chem. Phys.* **2008**, *129* (5), 054109-1-15.
(50) Frisch, M. J. T. G. W.; Schlegel, H. B.; Scuseria, G. E.; Robb, M. A.; Cheeseman, J. R.; Montgomery, J. A., Jr.; Vreven, T.; Kudin, K. N.; Burant, J. C.; et al. *Gaussian 03*, Revision C.02; Gaussian, Inc.: Wallingford, CT, 2004.
(51) Shi, Y. J.; Al-Basheer, W.; Thompson, R. I. *J. Chem. Phys.* **2009**, *130* (9), 094305-1-6.
(52) Lee, C. T.; Yang, W. T.; Parr, R. G. *Phys. Rev. B* **1988**, *37* (2), 785−789.
(53) Goedecker, S.; Maschke, K. *Phys. Rev. A* **1992**, *45* (1), 88−93.
(54) Forbert, H.; Kohlmeyer, A. *Fourier*, v 1.1; 2002−2008.
(55) Wannier, G. H. *J. Math. Phys.* **1978**, *19* (1), 131−134.
(56) Lapinski, L.; Nowak, M. J.; Kolos, R.; Kwiatkowski, J. S.; Leszczynski, J. *Spectrochim. Acta, A: Mol. Biomol. Spectrosc.* **1998**, *54A* (5), 685−693.
(57) Munshi, P.; Madsen, A. O.; Spackman, M. A.; Larsen, S.; Destro, R. *Acta Crystallogr., A* **2008**, *64* (Pt 4), 465−475.
(58) Ozaki, Y.; Futami, Y.; Ozaki, Y.; Hamada, Y.; Wojcik, M. J. *J. Phys. Chem. A* **2011**, *115* (7), 1194−1198.
(59) Wojcik, M. J.; Paluszkiewicz, C. *Can. J. Chem.* **1983**, *61* (7), 1449−1452.
(60) Wojcik, M. B. *Acad. Pol. Sci.—Chim.* **1974**, *22* (2), 71−73.
(61) Li, X.; Oomens, J.; Eyler, J. R.; Moore, D. T.; Iyengar, S. S. *J. Chem. Phys.* **2010**, *132* (24), 244301-1-15.
(62) Iyengar, S. S. *J. Chem. Phys.* **2005**, *123* (8), 084310-1-9.
(63) Iyengar, S. S. *J. Chem. Phys.* **2007**, *126* (21), 216101-1-2.
(64) Stare, J.; Mavri, J.; Grdadolnik, J.; Zidar, J.; Maksic, Z. B.; Vianello, R. *J. Phys. Chem. B* **2011**, *115* (19), 5999−6010.
(65) Nagel, Z. D.; Klinman, J. P. *Nat. Chem. Biol.* **2009**, *5* (8), 543−550.
(66) Warshel, A.; Olsson, M. H. M.; Mavri, J. *Philos. Trans. R. Soc. B* **2006**, *361* (1472), 1417−1432.
(67) Janezic, D.; Jezierska, A.; Panek, J.; Borstnik, U.; Mavri, J. *J. Phys. Chem. B* **2007**, *111* (19), 5243−5248.